

Coexistence of topological Anderson insulator and multifractal critical phase in a non-Hermitian quasicrystal

Qi-Bo Zeng^{1*} and Rong Lü^{2,3}

¹*Department of Physics, Capital Normal University, Beijing 100048, China*

²*State Key Laboratory of Low-Dimensional Quantum Physics,*

Department of Physics, Tsinghua University, Beijing 100084, China and

³*Collaborative Innovation Center of Quantum Matter, Beijing 100084, China*

The interplay of topology, disorder, and non-Hermiticity gives rise to phenomena beyond the conventional classification of quantum phases. We propose a one-dimensional non-Hermitian Su–Schrieffer–Heeger model with quasiperiodically modulated nonreciprocal intracell hopping. We show that quasiperiodic modulation can substantially enhance the topological regime and, remarkably, induce a non-Hermitian topological Anderson insulator (TAI) phase. Beyond the topological transition, increasing nonreciprocity drives a cascade of localization transitions in which all bulk eigenstates evolve from extended to multifractal critical and ultimately to localized states. Strikingly, the extended-to-critical transition coincides exactly with a real–complex spectral transition. We establish complete phase diagrams and derive exact analytical boundaries for both topological and localization transitions, uncovering an unanticipated coexistence of TAI and multifractal critical phases. Finally, we propose a feasible implementation in topoelectrical circuits. Our results reveal a new paradigm for studying the cooperative effects of topology, quasiperiodicity, and non-Hermiticity.

I. INTRODUCTION

The discovery of topological phases has fundamentally reshaped our understanding of quantum matter, revealing boundary states protected by global topological invariants [1–3]. While this framework was originally formulated for Hermitian systems, growing interest in open and dissipative platforms has propelled the development of non-Hermitian topology [4–7]. Non-Hermitian Hamiltonians naturally emerge in systems with gain and loss [8, 9], finite quasiparticle lifetimes [10], complex refractive indices in photonics [11, 12], and engineered Laplacians in electrical circuits [13–15]. In contrast to Hermitian counterparts, such systems host intrinsically non-Hermitian topological structures, including exceptional points [16] and complex-energy braiding [17–19]. Remarkably, they also support phases without Hermitian analogs [6, 7]. A defining feature of nonreciprocal systems is the breakdown of conventional bulk–boundary correspondence due to the non-Hermitian skin effect (NHSE), where an extensive number of eigenstates accumulate at the boundaries [20, 21]. The NHSE itself has a topological origin, intimately connected to point-gap topology under periodic boundary conditions [22–24].

Disorder, ubiquitous in realistic systems, generally destabilizes topological phases through Anderson localization [25]. Yet disorder can also play a constructive role: sufficiently strong randomness may induce topological transitions from trivial phases, leading to the topological Anderson insulator (TAI) [26–42]. The TAI phases and the topological properties based on the 1D Su–Schrieffer–Heeger (SSH) model with quasiperiodic disorders have also been studied extensively [43–48].

The interplay between disorder and non-Hermiticity further enriches localization and topological physics, producing unconventional phenomena that cannot be observed in the Hermitian systems [49–60]. Extending the TAI paradigm to non-Hermitian systems has revealed a diverse landscape of disorder-driven topological transitions [45, 61–64]. In parallel, quasiperiodic systems such as the André–Aubry–Harper model [65, 66] provide a deterministic route to localization transitions. With suitable quasiperiodic modulations or long-range hopping, quasicrystals can host mobility edges separating extended and localized states [67–71]. The associated critical states may proliferate into an intermediate multifractal phase, distinguished from both extended and localized regimes by its spectral statistics and wavefunction scaling properties [72–79]. Such critical phases are central to nonergodic dynamics, anomalous transport, and many-body localization phenomena [80–83]. Topological states in such quasiperiodic lattices have also been extensively investigated [84–92]. Despite these advances, a fundamental question remains unresolved: can a disorder-induced TAI phase and a multifractal critical phase coexist within a unified non-Hermitian quasiperiodic framework? To date, these phenomena have largely been treated as distinct regimes, and the conditions enabling their simultaneous emergence remain unknown.

In this work, we resolve this question by introducing a one-dimensional non-Hermitian SSH model with quasiperiodically modulated nonreciprocal intracell hopping. We show that quasiperiodicity not only enhances the robustness of the topological phase but also drives a disorder-induced transition into a non-Hermitian TAI phase. More strikingly, increasing nonreciprocity induces a cascade of localization transitions, with all bulk eigenstates evolving from extended to multifractal critical and ultimately to localized regimes. The extended-to-critical transition coincides exactly with a real–complex spectral

* zengqibo@cnu.edu.cn

transition, establishing a direct correspondence between spectral feature and wave-function criticality. By deriving exact analytical phase boundaries, we construct the complete phase diagram and uncover a previously unexplored regime where the TAI and multifractal critical phases coexist. Finally, we propose a feasible implementation of our model in topoelectrical circuits. Our work reveals the coexistence of a non-Hermitian TAI phase and a multifractal critical phase for all bulk states, where both the topological and the extended-critical-localized phase boundaries are analytically tractable. Hence our model provides an important platform to study the interplay of non-Hermiticity, topology, and quasiperiodic disorders.

The rest of the paper is organized as follows. In Sec. II, we will first introduce the model Hamiltonian of the 1D non-Hermitian SSH model with quasiperiodically modulated nonreciprocal intracell hopping. In Sec. III, we discuss the topological Anderson insulating phase and determine the phase boundaries. Then we will further investigate the extended-critical-localized phase transitions in Sec. IV. We also propose an experimental scheme for realizing the model in electric circuit in Sec. V. Finally in Sec. VI, we will summarize our results.

II. MODEL HAMILTONIAN

We consider a one-dimensional SSH chain with quasiperiodically modulated nonreciprocal intracell hopping, described by

$$H = H_{SSH} + H_\lambda, \quad (1)$$

with

$$\begin{aligned} H_{SSH} &= \sum_j \left(v c_{j,A}^\dagger c_{j,B} + w c_{j,B}^\dagger c_{j+1,A} + h.c. \right), \\ H_\lambda &= \sum_j \left(\lambda \cos \theta_j c_{j,A}^\dagger c_{j,B} - \lambda \cos \theta_j c_{j,B}^\dagger c_{j,A} \right). \end{aligned} \quad (2)$$

Here, $c_{j,A(B)}$ creates a spinless fermion on sublattice $A(B)$ of the j th unit cell. The parameters v and w denote the intracell and intercell hopping amplitudes, respectively, while λ characterizes the strength of nonreciprocity. The modulation phase $\theta_j = 2\pi\alpha j + \phi$ introduces spatial inhomogeneity; for irrational α , the nonreciprocity is quasiperiodic. Throughout this work we take $\alpha = (\sqrt{5} - 1)/2$, $\phi = 0$, and set $w = 1$ as the energy unit. The lattice contains N unit cells ($L = 2N$ sites), and all parameters are real.

The Hamiltonian takes a tridiagonal non-Hermitian form under open boundary conditions. For $|\lambda| < |v|$, it can be mapped to a Hermitian matrix via a similarity transformation $h = D^{-1}HD$ with diagonal D [93] (also see Appendix for details). Consequently, H is pseudo-Hermitian in the sense of Mostafazadeh [94], and its spectrum is entirely real in this regime. Due to the quasiperiodicity of the nonreciprocal hopping, there will be no skin

effect in this non-Hermitian model, and the spectra under open and periodic boundary conditions are consistent with each other [95]. As illustrated in Fig. 1(a) and 1(b), the eigenenergies remain real for $|\lambda| < |v|$ under periodic boundary conditions, while a real-complex spectral transition occurs at $|\lambda| = |v|$, beyond which the similarity transformation breaks down and complex eigenvalues emerge.

To analyze the localization induced by quasiperiodic nonreciprocity, we formulate the transfer-matrix approach and compute the Lyapunov exponent. From the stationary Schrödinger equation $H|\psi\rangle = E|\psi\rangle$, with eigenstate $|\psi\rangle = \sum_j a_j|j, A\rangle + b_j|j, B\rangle$, yields

$$\begin{cases} E a_j = (v + \lambda \cos \theta_j) b_j + w b_{j-1}, \\ E b_j = (v - \lambda \cos \theta_j) a_j + w a_{j+1}. \end{cases} \quad (3)$$

Introducing the two-component vector

$$\Psi_j = \begin{pmatrix} a_j \\ b_{j-1} \end{pmatrix}, \quad (b_0 = 0), \quad (4)$$

the recursion relation can be written as

$$\Psi_{j+1} = T_E(\theta_j) \Psi_j, \quad (5)$$

with transfer matrix

$$T_E(\theta_j) = \frac{1}{w(v + \lambda \cos \theta_j)} \begin{pmatrix} E^2 - (v^2 - \lambda^2 \cos^2 \theta_j) & -Ew \\ Ew & -w^2 \end{pmatrix}. \quad (6)$$

The Lyapunov exponent is defined as

$$\gamma(E) = \lim_{N \rightarrow \infty} \frac{1}{N} \ln \left\| \prod_{j=1}^N T_E(\theta_j) \right\|, \quad (7)$$

where N is the number of unit cells and $\|\cdot\|$ denotes the matrix norm. The localization length is given by $\xi = \gamma^{-1}(E)$; thus $\gamma(E) > 0$ signals localized state, while $\gamma(E) = 0$ corresponds to extended or critical state.

To numerically characterize the localization features of the eigenstates, we can also compute the moments $I_q(n) = \sum_{j,\alpha} |\psi_{nR,j\alpha}|^{2q} \propto L^{-D_q(q-1)}$ with $\alpha = A$ and B , where $\psi_{nR,j\alpha}$ is the j th component on sublattice α of the n th right eigenstate $|\psi_{nR}\rangle$ and D_q are the fractal dimensions. q is a positive integer. If the eigenstates are localized (extended), we have $D_q \rightarrow 0$ (1). While for the multifractal states, we have $0 < D_q < 1$ [70, 96]. Taking $q = 2$ in I_q , we obtain the famous inverse participation ratio (IPR) as $\text{IPR}(\psi_{nR}) = \sum_{j,\alpha} |\psi_{nR,j\alpha}|^4$ and fractal dimension as $D_2(\psi_{nR}) = -\lim_{L \rightarrow \infty} [\ln \text{IPR}(\psi_{nR}) / \ln L]$, which are extensively used to characterize the localization properties. In the thermodynamic limit, $\text{IPR}(\psi_{nR}) \rightarrow 0$ for extended states and remains finite for localized states.

III. TOPOLOGICAL ANDERSON INSULATOR

For the clean SSH model ($\lambda = 0$), the system is topologically nontrivial when $|v| < |w|$. Introducing

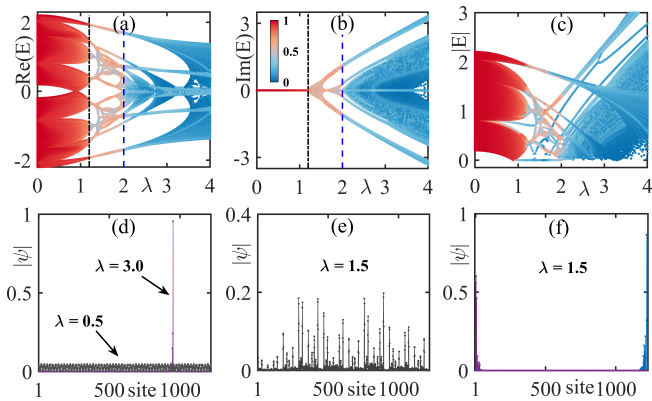


FIG. 1. (Color online) (a) Real and (b) imaginary parts of the eigenenergies under periodic boundary conditions as a function of the nonreciprocity strength λ . The black and blue dashed lines mark the critical values $\lambda = v$ and $\lambda = 2w$, separating the extended, multifractal critical, and localized regimes. The color scale indicates the fractal dimension of the corresponding eigenstates. (c) Energy spectrum $|E|$ under open boundary conditions. (d)–(e) Representative spatial profiles of eigenstates in the extended, critical, and localized phases, respectively. (f) Zero-energy edge modes in the topological Anderson insulating phase. Parameters: $v = 1.2$, $w = 1$, and system size $L = 2N = 1220$.

quasiperiodic nonreciprocity fundamentally alters this criterion. Remarkably, we find that a topological phase can emerge in the parameter regime that is trivial in the clean limit, thereby realizing a non-Hermitian topological Anderson insulator (TAI). Figure 1(c) shows the open-boundary spectrum $|E|$ as a function of λ when $v = 1.2 > w$, where the clean system is topologically trivial. As λ increases, zero-energy modes appear within a finite parameter window. Their spatial profiles [Fig. 1(f)] reveal two states exponentially localized at opposite ends of the chain, confirming the onset of a nontrivial topological phase induced by quasiperiodic nonreciprocity.

The topological transition can be determined analytically from the divergence of the localization length of the zero-energy modes. Setting $E = 0$ in Eq. (3), the two equations decouple and yield

$$a_{j+1} = -\frac{v - \lambda \cos \theta_j}{w} a_j. \quad (8)$$

Iterating from $j = 1$ to $j = N$ gives

$$a_{N+1} = (-1)^N \prod_{j=1}^N \frac{v - \lambda \cos \theta_j}{w} a_1. \quad (9)$$

The Lyapunov exponent for the zero-energy mode is therefore

$$\gamma(0) = \lim_{N \rightarrow \infty} \frac{1}{N} \sum_{j=1}^N \ln \left| \frac{v - \lambda \cos \theta_j}{w} \right|. \quad (10)$$

Since $\theta_j = 2\pi\alpha j + \phi$ with irrational α , Weyl's equidistribution theorem ensures that the sequence is uniformly

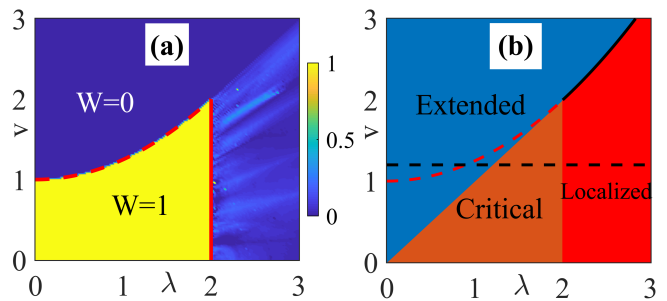


FIG. 2. (Color online) (a) Phase diagram in the $v - \lambda$ plane showing the topologically nontrivial ($W = 1$) and trivial ($W = 0$) phases. The color scale represents the real-space winding number W . Red dashed and solid lines denote the analytical phase boundaries given by Eq. (13). (b) Phase diagram of the extended, multifractal critical, and localized regimes determined from the Lyapunov exponent and fractal dimension. The red dashed line is the same as in (a). The black solid line is the phase boundary separating the extended and localized phase. The black dashed line indicates the cut at $v = 1.2$.

distributed on $[0, 2\pi)$, The Lyapunov exponent reduces to the phase average [53, 97, 98]

$$\gamma(0) = \frac{1}{2\pi} \int_0^{2\pi} \ln \left| \frac{v - \lambda \cos \theta}{w} \right| d\theta. \quad (11)$$

Using Jensen's formula, the integral can be evaluated exactly, yielding

$$\gamma(0) = \begin{cases} \ln \frac{|v| + \sqrt{v^2 - \lambda^2}}{2|w|}, & |\lambda| < |v|; \\ \ln \frac{|\lambda|}{2|w|}, & |\lambda| \geq |v|. \end{cases} \quad (12)$$

The topological phase boundaries follow from $\gamma_0 = 0$,

$$\begin{cases} |v| + \sqrt{v^2 - \lambda^2} = 2|w| & |\lambda| < |v|; \\ |\lambda| = |2w|, & |\lambda| \geq |v|. \end{cases} \quad (13)$$

These expressions provide exact analytical criteria for the disorder-induced topological phase transition.

To further characterize the topological phase, we compute the real-space winding number under open boundary conditions [99]. The Hamiltonian preserves chiral symmetry, $SHS^{-1} = -H$, with $S = \sigma_z \otimes \mathcal{I}$. Let $|\psi_{nR}^\pm\rangle$ and $|\psi_{nL}^\pm\rangle$ denote the biorthonormal right and left eigenstates, which respectively satisfy the Schrödinger equations $H|\psi_{nR}^\pm\rangle = \pm E_n|\psi_{nR}^\pm\rangle$ and $H^\dagger|\psi_{nL}^\pm\rangle = \pm E_n^*|\psi_{nL}^\pm\rangle$. Excluding edge modes, we define the open-boundary Q matrix as $Q = \sum_n (|\psi_{nR}^+\rangle\langle\psi_{nL}^+| - |\psi_{nR}^-\rangle\langle\psi_{nL}^-|)$, and the winding number

$$W = \frac{1}{2L'} \text{Tr}'(SQ[Q, X]), \quad (14)$$

where X is the coordinate operator and Tr' denotes the trace over a central region of length L' . In this work, we have taken the central region with $N/2 \leq n \leq 3N/2$ such that $L' = N$ in the numeric implementation. We

find $W = 1$ in the topologically nontrivial regime and $W = 0$ in the trivial regime.

The resulting phase diagram in the $v-\lambda$ plane is shown in Fig. 2(a). We can see that in the region with $1 < v < 2$, the system is trivial when the disorder is weak. As λ increases, the system will enter into the nontrivial phase with $W = 1$, this is the topological Anderson insulating phase induced by the nonreciprocal quasiperiodic disorder. When λ further increases, the system will become trivial again at $\lambda = 2$. The boundaries separating the blue and yellow regions with different winding numbers, which are numerically obtained, agree precisely with the analytical boundaries in Eq. (13), as indicated by the red dashed and solid lines in Fig. 2(a), confirming the emergence of a disorder-induced topological phase.

IV. EXTENDED-CRITICAL-LOCALIZED PHASE TRANSITIONS

Quasiperiodic nonreciprocity also drives Anderson-type localization transitions. As shown in Figs. 1(a) and 1(b), the spectrum separates into three distinct regimes characterized by the fractal dimension Γ of the eigenstates. For $v = 1.2$, all states are extended when $|\lambda| < 1.2$, become multifractal critical in the intermediate region $1.2 < |\lambda| < 2$, and are fully localized for $|\lambda| > 2$. Representative wave-function profiles are displayed in Figs. 1(d) and 1(e), where the critical states exhibit clear multifractal spatial structures.

To quantify the transition, we compute the average values of the inverse participation ratio and fractal dimension, which are respectively defined as $\langle IPR \rangle = \sum_n [IPR(\psi_{nR})]/L$ and $\langle D_2 \rangle = \sum_n [D_2(\psi_{nR})]/L$. Figure 3(a) and 3(b) show their dependence on λ for different system sizes under periodic boundary conditions, such that the influences of topological edge modes are excluded. In the extended regime, $\langle IPR \rangle \rightarrow 0$ and $\langle D_2 \rangle \rightarrow 1$ as L increases, while in the localized regime $\langle IPR \rangle$ remains finite and $\langle D_2 \rangle \rightarrow 0$. In contrast, both quantities remain taking intermediate values in the critical regime, and the $\langle D_2 \rangle$ behaves independently with the system size, consistent with multifractal scaling. Figure 3(c) further plots the D_2 values of all eigenstates, where the color indicates the fractal dimensions of eigenstates. We can see that there is no mobility edges in the spectrum, and the boundaries indicated by the color scale at $\lambda = 1.2$ and 2 are quite clear, consistent with the results presented in Fig. 3(a) and 3(b). For the multifractal critical phase, we further calculate the D_q values of three representative eigenstates: $n = 1, 300$, and 610 , with q varying from 2 to 10 , as shown in Fig. 3(d). We can see that the D_q values are q dependent, but always remain a finite value satisfying $0 < D_q < 1$, as expected for the multifractal states.

The localization transition can be determined analytically by using Avila's global theory for quasiperiodic cocycles [100, 101]. For the case with $|\lambda| < |v|$, the transfer

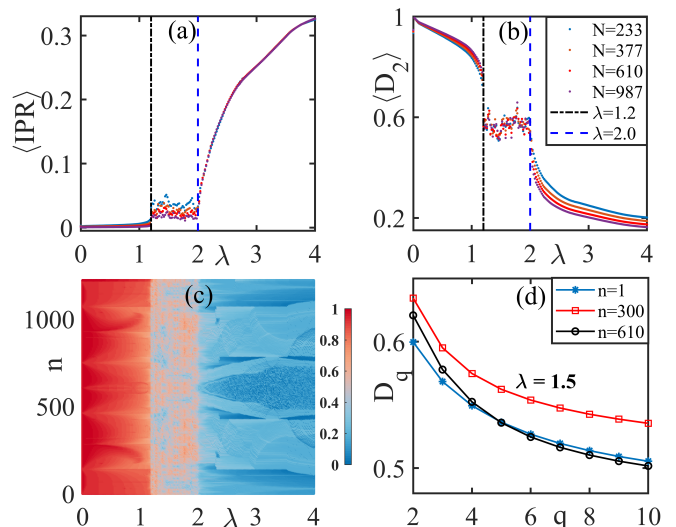


FIG. 3. (Color online) (a) Average value of the inverse participation ratio $\langle IPR \rangle$ and (b) average value of the fractal dimension $\langle D_2 \rangle$ as functions of the nonreciprocity strength λ for different system sizes under periodic boundary conditions. The black dot-dashed and blue dashed lines mark the analytical phase boundaries separating the extended-critical and critical-localized regimes, respectively. (c) shows the D_2 values of all the eigenstates of the system with $N = 610$, which are indicated by the color scale. (d) Fractal dimensions D_q for the 1st, 300th, and 610th eigenstate at $\lambda = 1.5$ in (c) as a function of q . Parameters: $v = 1.2$ and $w = 1$.

matrix defines an analytic cocycle $(\alpha, T_E(\theta))$. However, if $|\lambda| \geq |v|$, the transfer matrix in Eq. (6) will become singular due to the $(v + \lambda \cos \theta_j)$ term in the denominator and the cocycle $(\alpha, T_E(\theta))$ also becomes singular. Since the Avila's global theory is developed to one-frequency analytic cocycles [100], we need to extend it to deal with the singular case here. To do so, we define the following new transfer matrix

$$\tilde{T}_E(\theta_j) = (v + \lambda \cos \theta_j) T_E(\theta_j). \quad (15)$$

Then the N -step transfer matrix is $\tilde{\mathcal{T}}_N = \left[\prod_{j=1}^N (v + \lambda \cos \theta_j) \right] \mathcal{T}_N$, with $\mathcal{T}_N = \prod_{j=1}^N T_E(\theta_j)$, and we have

$$\ln \left\| \tilde{\mathcal{T}}_N \right\| = \sum_{j=1}^N \ln |v + \lambda \cos \theta_j| + \ln \|\mathcal{T}_N\|. \quad (16)$$

According to the definition of Lyapunov exponent in Eq. (7), the above formula leads to

$$\tilde{\gamma}(E) = \gamma(E) + \lim_{N \rightarrow \infty} \frac{1}{N} \sum_{j=1}^N \ln |v + \lambda \cos \theta_j|. \quad (17)$$

Since $\tilde{T}_E(\theta_j)$ is analytic, the transfer matrix defines an analytic $SL(2, \mathcal{R})$ cocycle, which is denoted as

($\alpha, \tilde{T}_E(\theta_j)$). Then we can use the Avila's theory to compute the $\tilde{\gamma}(E)$. Due to the ergodicity, the Lyapunov exponent admits a phase-averaged representation

$$\tilde{\gamma}(E) = \lim_{N \rightarrow \infty} \frac{1}{2\pi N} \int_0^{2\pi} \ln \left\| \tilde{T}_E(\theta_j) \right\| d\theta. \quad (18)$$

By replacing θ with $\theta + iy$ with $y \in \mathcal{R}$, we get the complexified Lyapunov exponent and have

$$\gamma(E, y) = \tilde{\gamma}(E, y) - \int_0^{2\pi} \ln |v + \lambda \cos(\theta + iy)| \frac{d\theta}{2\pi}. \quad (19)$$

Setting $I(y) = \int_0^{2\pi} \ln |v + \lambda \cos(\theta + iy)| \frac{d\theta}{2\pi}$, one has

$$I(y) = \begin{cases} \ln \frac{|v + \sqrt{v^2 - \lambda^2}|}{2}, & |\lambda| < |v|; \\ |y| + \ln \frac{|\lambda|}{2}, & |\lambda| \geq |v|. \end{cases} \quad (20)$$

Now since $\tilde{T}_E(\theta_j)$ is analytic, Avila's global theory ensures that $\tilde{\gamma}(E, y)$ is a continuous, convex, piecewise linear function with respect to y . For large $|y|$, the term $\lambda \cos(\theta + iy)$ behaves as

$$\lambda \cos(\theta + iy) \sim \frac{\lambda}{2} e^{|y|} e^{\pm i\theta}. \quad (21)$$

In this limit, the transfer matrix becomes asymptotically triangular. Consequently, for the Lyapunov exponent $\tilde{\gamma}(E, y)$, we have

$$\tilde{\gamma}(E, y) = 2|y| + \ln \left| \frac{\lambda^2}{4w} \right| + o(1), \quad (22)$$

where $o(1) \rightarrow 0$ in the large $|y|$ limit. This leads to

$$\gamma(E, y) = 2|y| + \ln \left| \frac{\lambda^2}{4w} \right| - I(y), \quad (23)$$

and we have

$$\gamma(E, y) = \begin{cases} 2|y| + \ln \frac{|v - \sqrt{v^2 - \lambda^2}|}{2|w|}, & |\lambda| < |v|; \\ |y| + \ln \left| \frac{\lambda}{2w} \right|, & |\lambda| \geq |v|. \end{cases} \quad (24)$$

The physical Lyapunov exponent corresponds to $\gamma(E, 0)$.

From Avila's global theory, the physical Lyapunov exponent is obtained by matching the asymptotic behavior at large $|y|$, which gives

$$\gamma(E) = \begin{cases} \max \left\{ 0, \ln \frac{|v - \sqrt{v^2 - \lambda^2}|}{2|w|} \right\}, & |\lambda| < |v|; \\ \max \left\{ 0, \ln \left| \frac{\lambda}{2w} \right| \right\}, & |\lambda| \geq |v|. \end{cases} \quad (25)$$

Remarkably, $\gamma(E)$ is independent of E . Therefore, all bulk states share the same localization behavior, and no mobility edge appears in the spectrum. If $\gamma(E) = 0$, the system is in the extended or critical phase; while if $\gamma(E) > 0$, the system is in the localized phase. The phase boundaries can be determined from the above formula by setting $\gamma(E) = 0$, which leads to two critical lines

$$|\lambda_{c1}| = 2|w| \sqrt{\left| \frac{v}{w} \right| - 1}, \quad \text{and} \quad |\lambda_{c2}| = 2|w|, \quad (26)$$

which coincides at $|v| = 2|w|$.

Note that if $|\lambda| < |v| < 2|w|$, $\ln \frac{|v - \sqrt{v^2 - \lambda^2}|}{2|w|} < 0$, then according to Eq. (25), $\gamma(E) = 0$ will always hold, implying that the system will in the extended or critical phase in this regime. On the other hand, if $|v| \leq |\lambda| < 2|w|$, $\gamma(E)$ is determined by $\ln \left| \frac{\lambda}{2w} \right|$, then the critical disorder strength is $|\lambda_{c2}| = 2|w|$. Thus, when $|\lambda| < 2|w|$, $\gamma(E) = 0$, the system is in the extended or critical phase. If $|\lambda| > 2|w|$, $\gamma(E) > 0$, and all eigenstates are localized. The distinction between extended and critical phases is controlled by the competition between v and λ . When $|\lambda| < |v|$, the spectrum is absolutely continuous and all states are extended. For $|v| < |\lambda| < 2|w|$, the spectrum becomes singular continuous [102], and all eigenstates are multifractal. Physically, the critical regime originates from incommensurate zeros in the effective hopping amplitudes when $|\lambda| > |v|$ [103, 104]. So, for the region with $|v| < 2|w|$, the system therefore exhibits three different phases

$$\begin{cases} \text{extended phase:} & 0 < |\lambda| < |v|, \\ \text{critical phase:} & |v| < |\lambda| < 2|w|, \\ \text{localized phase:} & |\lambda| > 2|w|. \end{cases} \quad (27)$$

The resulting phase diagram is shown in Fig. 2(b). Comparing with the topological phase diagram in Fig. 2(a), we uncover a finite parameter region where the topologically nontrivial phase overlaps with the multifractal critical regime. Along the representative cut $v = 1.2$, as indicated by the black dashed line in Fig. 2(b), the system evolves as follows: starting from a trivial extended phase at $\lambda = 0$, increasing λ first induces a TAI phase with extended bulk states; further increasing λ drives the bulk into a multifractal critical phase while the zero-energy edge modes persist; finally, for $|\lambda| > 2|w|$, the system becomes localized and topologically trivial. Notably, the extended-critical phase transition at $|\lambda| = |v|$ coincides exactly with the real-complex spectral transition, establishing a direct correspondence between the spectral property and wave-function criticality. Moreover, the critical window shrinks as $|v|$ increases and disappears entirely when $|v| > 2|w|$.

For the regime $|v| > 2|w|$, the system exhibits the following two phases

$$\begin{cases} \text{extended phase:} & 0 < |\lambda| < 2|w| \sqrt{\left| \frac{v}{w} \right| - 1}, \\ \text{localized phase:} & |\lambda| > 2|w| \sqrt{\left| \frac{v}{w} \right| - 1}, \end{cases} \quad (28)$$

which are separated by $|\lambda_{c1}|$. This phase boundary is plotted in Fig. 2(b), as indicated by the black solid line separating the blue and red region.

Above we have analytically determined the phase boundaries for the extended-critical-localized phases in the SSH model nonreciprocal quasiperiodic intracell hopping by extending the Avila's theory, the results are in good agreement with the numeric calculations. We also reveal the coexistence of multifractal critical phase and

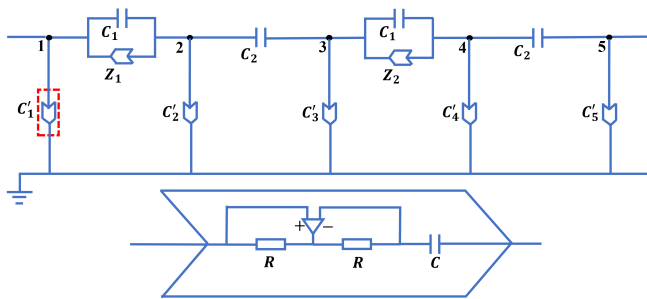


FIG. 4. (Color online) Schematic of the topoelectrical circuit realizing the non-Hermitian quasicrystal. The numbered black nodes represent lattice sites of the SSH chain. Capacitive couplings implement the Hermitian hopping terms, while the element highlighted in red denotes a negative-impedance converter with current inversion (INIC), which generates direction-dependent (nonreciprocal) intracell hopping. The effective impedances Z_j and Z'_j are controlled by the orientation of the INIC. The lower panel illustrates the internal structure of the INIC, whose impedance depends on the direction of the current flow.

the nontrivial TAI phase induced by the nonreciprocal quasiperiodic modulation in the model, which have not been reported before.

V. EXPERIMENTAL SCHEME IN ELECTRIC CIRCUITS

Topoelectrical circuits have emerged as a versatile platform for simulating topological band structures and non-Hermitian phenomena [13–15]. We propose a circuit implementation of the non-Hermitian quasicrystal, schematically shown in Fig. 4. In the circuit network, nodes represent lattice sites of the SSH chain. The capacitors C_1 and C_2 realize the intra- and intercell hopping amplitudes, respectively. Nonreciprocal intracell

hopping is implemented using negative-impedance converters with current inversion (INICs), whose direction-dependent impedance Z_j generates the asymmetric hopping terms. By appropriately designing Z_j s and Z'_j , the circuit Laplacian \mathbf{J} defined through $\mathbf{I} = \mathbf{J}\mathbf{V}$ (with \mathbf{I} and \mathbf{V} the nodal current and voltage vectors), reproduces the effective Hamiltonian in Eq. (1) (see Appendix). Topological and localization properties can be probed via impedance measurements. In particular, zero-energy edge modes manifest as pronounced peaks in the two-point impedance at the boundaries, while the admittance spectrum directly reveals the real–complex spectral transition and the localization regimes predicted in this work.

VI. SUMMARY

We have introduced and analytically characterized a non-Hermitian SSH quasicrystal with quasiperiodically modulated nonreciprocity. The interplay between non-Hermiticity and quasiperiodicity gives rise to two intertwined phenomena: a disorder-induced non-Hermitian TAI and a cascade of extended–critical–localized transitions. Most notably, we uncover a finite parameter regime where the TAI phase coexists with a multifractal critical bulk—an effect absent in previously studied disordered topological systems. We establish exact analytical phase boundaries and demonstrate that the extended–critical transition coincides precisely with the real–complex spectral transition, revealing a direct correspondence between spectral feature and wave-function criticality. The proposed topoelectrical circuit implementation offers an experimentally accessible route to probe these multifractal topological states. More broadly, quasiperiodic nonreciprocity provides a general mechanism for engineering hybrid quantum phases in which topology, non-Hermiticity, and criticality are intrinsically intertwined.

APPENDIX

A. The condition for a real spectrum

Under open boundary conditions, the model Hamiltonian in Eq. (1) can be written as a tridiagonal matrix describing a one-dimensional nonreciprocal lattice. Defining the nearest-neighbor hopping amplitudes

$$t_{2j-1} = v + \lambda \cos \theta_j, \quad t'_{2j-1} = v - \lambda \cos \theta_j, \quad t_{2j} = t'_{2j} = w, \quad (\text{A1})$$

where t_n (t'_n) is the backward (forward) hopping amplitude between the n th and the $(n+1)$ th lattice sites. The Hamiltonian takes the form

$$H = \begin{pmatrix} 0 & t_1 & 0 & 0 & \cdots & 0 \\ t'_1 & 0 & t_2 & 0 & \cdots & 0 \\ 0 & t'_2 & 0 & t_3 & \cdots & 0 \\ 0 & 0 & t'_3 & 0 & t_4 & \cdots \\ \vdots & \vdots & \vdots & \vdots & \ddots & \vdots \\ 0 & 0 & 0 & 0 & \cdots & 0 \end{pmatrix} = \begin{pmatrix} 0 & v + \lambda \cos \theta_1 & 0 & 0 & \cdots & 0 \\ v - \lambda \cos \theta_1 & 0 & w & 0 & \cdots & 0 \\ 0 & w & 0 & v + \lambda \cos \theta_2 & \cdots & 0 \\ 0 & 0 & v - \lambda \cos \theta_2 & 0 & w & \cdots \\ \vdots & \vdots & \vdots & \vdots & \ddots & \vdots \\ 0 & 0 & 0 & 0 & \cdots & 0 \end{pmatrix}. \quad (\text{A2})$$

All the elements in the matrix are real and we have $t_j \neq t'_j$, implying that the matrix is non-Hermitian.

Assume that $t_j t'_j > 0$, we construct a diagonal matrix

$$D = \begin{pmatrix} d_1 & 0 & 0 & 0 & \cdots & 0 \\ 0 & d_2 & 0 & 0 & \cdots & 0 \\ 0 & 0 & d_3 & 0 & \cdots & 0 \\ 0 & 0 & 0 & d_4 & 0 & \cdots \\ \vdots & \vdots & \vdots & \vdots & \ddots & \vdots \\ 0 & 0 & 0 & 0 & \cdots & d_L \end{pmatrix}, \quad (\text{A3})$$

with

$$d_n = \begin{cases} 1, & j = 1 \\ \sqrt{\frac{t'_{n-1} t'_{n-2} \cdots t'_1}{t_{n-1} t_{n-2} \cdots t_1}}, & n = 2, 3, \dots, L \end{cases} \quad (\text{A4})$$

Under the similarity transformation $h = D^{-1} H D$, the Hamiltonian becomes

$$h = \begin{pmatrix} 0 & \text{sgn}(t_1) \sqrt{t_1 t'_1} & 0 & 0 & \cdots & 0 \\ \text{sgn}(t_1) \sqrt{t_1 t'_1} & 0 & \text{sgn}(t_2) \sqrt{t_2 t'_2} & 0 & \cdots & 0 \\ 0 & \text{sgn}(t_2) \sqrt{t_2 t'_2} & 0 & \text{sgn}(t_3) \sqrt{t_3 t'_3} & \cdots & 0 \\ 0 & 0 & \text{sgn}(t_3) \sqrt{t_3 t'_3} & 0 & \text{sgn}(t_4) \sqrt{t_4 t'_4} & \cdots \\ \vdots & \vdots & \vdots & \vdots & \ddots & \vdots \\ 0 & 0 & 0 & 0 & \cdots & 0 \end{pmatrix}. \quad (\text{A5})$$

Because condition $t_j t'_j > 0$ guarantees, all square roots are real and h is Hermitian. Since similarity transformations preserve the spectrum, H and h share identical eigenvalues. Therefore, the spectrum of H is entirely real whenever the condition $t_j t'_j > 0$ holds.

For the present model,

$$t_{2j-1} t'_{2j-1} = (v + \lambda \cos \theta_j)(v - \lambda \cos \theta_j) = v^2 - \lambda^2 \cos^2 \theta_j. \quad (\text{A6})$$

The condition $t_j t'_j > 0$ for all j requires

$$v^2 - \lambda^2 \cos^2 \theta_j > 0 \quad \forall j, \quad (\text{A7})$$

which is satisfied if and only if

$$|\lambda| < |v|. \quad (\text{A8})$$

Thus, the critical point for the real-to-complex spectral transition is

$$|\lambda| = |v|. \quad (\text{A9})$$

For $|\lambda| > |v|$, the similarity transformation breaks down because some t_n and t'_n become negative, and complex eigenvalues necessarily emerge.

The above similarity transformation implies that the Hamiltonian is pseudo-Hermitian. Indeed,

$$D^2 H^\dagger D^{-2} = D^2 (D h D^{-1})^\dagger D^{-2} = D h D^{-1} = H, \quad (\text{A10})$$

which yields $H^\dagger = \eta^{-1} H \eta$ with $\eta = D^2$. Thus, the Hamiltonian is pseudo-Hermitian. Therefore, H is pseudo-Hermitian and admits a real spectrum in the parameter regime $|\lambda| < |v|$.

Notably, this argument does not depend on the specific functional form of t_n and applies generally to one-dimensional nonreciprocal tridiagonal Hamiltonians [93].

B. Experimental scheme using topoelectrical circuits

The non-Hermitian quasicrystal proposed in the main text can be experimentally realized using topoelectrical circuits, which have emerged as a versatile platform for simulating non-Hermitian band structures and topological phases. The circuit configuration is shown in Fig. 4 of the main text. The numbered black dots denote circuit nodes corresponding to lattice sites, where external voltage sources or impedance measurements can be applied.

The circuit consists of capacitors and negative-impedance converters with current inversion (INICs), which generate direction-dependent couplings and thereby emulate nonreciprocal hopping. The INIC structure (lower panel of Fig. 4) comprises two resistors, one capacitor, and an operational amplifier. Importantly, its effective impedance depends on the direction of current flow: it behaves as a negative capacitance for one orientation and as a positive capacitance for the opposite orientation, thus realizing asymmetric hopping amplitudes.

For a node j in the circuit, let I_j and V_j denote the input current and voltage, respectively. Kirchhoff's current law gives

$$I_j = \sum_i Y_{ji}(V_j - V_i) + X_j V_j, \quad (\text{A11})$$

where Y_{ji} is the admittance between nodes j and i , and X_j denotes the shunt admittance at node j . Collecting all nodes, the voltage-current relation takes the matrix form

$$\mathbf{I} = \mathbf{J}\mathbf{V}, \quad (\text{A12})$$

where \mathbf{J} is the circuit Laplacian. The circuit Laplacian can be used to model the tight-binding lattices Hamiltonian.

For the electrical circuit shown in Fig. (4), the Laplacian is

$$\mathbf{J} = i\omega \begin{pmatrix} C_1 + Z_1 - C'_1 & -(C_1 + Z_1) & 0 & 0 & 0 & \cdots \\ -(C_1 - Z_1) & C_1 + C_2 - Z_1 - C'_2 & -C_2 & 0 & 0 & \cdots \\ 0 & -C_2 & C_1 + C_2 + Z_2 - C'_3 & -(C_1 + Z_2) & 0 & \cdots \\ 0 & 0 & -(C_1 - Z_2) & C_1 + C_2 - Z_2 - C'_4 & -C_2 & \cdots \\ \vdots & \vdots & \vdots & \vdots & \ddots & \vdots \\ 0 & 0 & 0 & 0 & \cdots & C_1 - Z_N - C'_L \end{pmatrix}. \quad (\text{A13})$$

This structure reproduces the tight-binding Hamiltonian under open boundary conditions, up to the overall factor $i\omega$.

To eliminate the diagonal (on-site) terms and obtain a purely off-diagonal SSH-type structure, we choose

$$C'_1 = C_1 + Z_1, \quad C'_L = C_1 - Z_N, \quad C'_{2j} = C_1 + C_2 - Z_j \quad C'_{2j-1} = C_1 + C_2 + Z_j \quad \text{for } 1 < j < N. \quad (\text{A14})$$

The Laplacian then reduces to

$$\mathbf{J} = i\omega \begin{pmatrix} 0 & -(C_1 + Z_1) & 0 & 0 & 0 & \cdots \\ -(C_1 - Z_1) & 0 & -C_2 & 0 & 0 & \cdots \\ 0 & -C_2 & 0 & -(C_1 + Z_2) & 0 & \cdots \\ 0 & 0 & -(C_1 - Z_2) & 0 & -C_2 & \cdots \\ \vdots & \vdots & \vdots & \vdots & \ddots & \vdots \\ 0 & 0 & 0 & 0 & \cdots & 0 \end{pmatrix}. \quad (\text{A15})$$

Identifying

$$C_1 \leftrightarrow v, \quad C_2 \leftrightarrow w, \quad Z_j = \lambda \cos(2\pi\alpha j + \phi), \quad (\text{A16})$$

the circuit Laplacian becomes directly proportional to the non-Hermitian quasicrystal Hamiltonian discussed in the main text.

The admittance spectrum of the circuit corresponds to the energy spectrum of the Hamiltonian. In particular, zero-admittance resonances signal topological edge modes. The energy spectrum is obtained from the admittance spectrum of the circuit and can be used to detect the spectral properties reported in this work.

ACKNOWLEDGMENTS

This work is supported by the National Natural Science Foundation of China (Grant No. 12204326). R.L.

is supported by the Quantum Science and Technology-

National Science and Technology Major Project (Grant No. 2021ZD0302100) and the 'Gravitational Wave De-

tection' program (2023YFC2205800) funded by the Ministry of Science and Technology of the People's Republic of China.

-
- [1] M. Z. Hasan and C. L. Kane, Colloquium: Topological insulators, *Rev. Mod. Phys.* **82**, 3045 (2010).
- [2] X.-L. Qi and S.-C. Zhang, Topological insulators and superconductors, *Rev. Mod. Phys.* **83**, 1057 (2011).
- [3] N. P. Armitage, E. J. Mele, and A. Vishwanath, Weyl and Dirac semimetals in three-dimensional solids, *Rev. Mod. Phys.* **90**, 015001 (2018).
- [4] H. Cao and J. Wiersig, Dielectric microcavities: Model systems for wave chaos and non-Hermitian physics, *Rev. Mod. Phys.* **87**, 61 (2015).
- [5] V. V. Konotop, J. Yang, and D. A. Zezyulin, Nonlinear waves in PT-symmetric systems, *Rev. Mod. Phys.* **88**, 035002 (2016).
- [6] Y. Ashida, Z. Gong, and M. Ueda, Non-Hermitian physics, *Adv. Phys.* **69**, 249 (2020).
- [7] E. J. Bergholtz, J. C. Budich, and F. K. Kunst, Exceptional topology of non-Hermitian systems, *Rev. Mod. Phys.* **93**, 015005 (2021).
- [8] C. M. Bender and S. Boettcher, Real spectra in non-Hermitian Hamiltonians having PT symmetry, *Phys. Rev. Lett.* **80**, 5243 (1998).
- [9] C. M. Bender, Making sense of non-Hermitian Hamiltonians, *Rep. Prog. Phys.* **70**, 947 (2007).
- [10] V. Kozii and L. Fu, Non-Hermitian topological theory of finite-lifetime quasiparticles: prediction of bulk Fermi arc due to exceptional point, [arXiv:1708.05841](https://arxiv.org/abs/1708.05841).
- [11] Z. H. Musslimani, K. G. Makris, R. El-Ganainy, and D. N. Christodoulides, Optical solitons in PT periodic potentials, *Phys. Rev. Lett.* **100**, 030402 (2008).
- [12] L. Feng, R. El-Ganainy, and L. Ge, Non-Hermitian photonics based on parity-time symmetry, *Nat. Photonics* **11**, 752 (2017).
- [13] K. F. Luo, J. J. Feng, Y. X. Zhao, and R. Yu, Nodal manifolds bounded by exceptional points on non-Hermitian honeycomb lattices and electrical-circuit realization, [arXiv:1810.09231](https://arxiv.org/abs/1810.09231).
- [14] C. H. Lee, S. Imhof, C. Berger, F. Bayer, J. Brehm, L. W. Molenkamp, T. Kiessling, and R. Thomale, Topoelectrical circuits, *Commun. Phys.* **1**, 39 (2018).
- [15] H. Sahin, M. B. A. Jalil, C. H. Lee, Topoelectrical circuits-recent experimental advances and developments, [arXiv:2502.18563](https://arxiv.org/abs/2502.18563).
- [16] W. D. Heiss, The physics of exceptional points, *J. Phys. A: Math. Theor.* **45**, 444016 (2012).
- [17] H. Hu and E. Zhao, Knots and non-Hermitian Bloch bands, *Phys. Rev. Lett.* **126**, 010401 (2021).
- [18] K. Wang, A. Dutt, C. C. Wojcik, and S. Fan, Topological complex-energy braiding of non-Hermitian bands, *Nature* **598**, 59 (2021).
- [19] Z. Zhou, Z.-C. Xu, and L.-J. Lang, Non-Abelian geometry, topology, and dynamics of a nonreciprocal Su-Schrieffer-Heeger ladder, *Phys. Rev. B* **112**, 094305 (2025).
- [20] S. Yao and Z. Wang, Edge states and topological invariants of non-Hermitian systems, *Phys. Rev. Lett.* **121**, 086803 (2018).
- [21] S. Yao, F. Song, and Z. Wang, Non-Hermitian Chern bands, *Phys. Rev. Lett.* **121**, 136802 (2018).
- [22] Dan S. Borgnia, Alex Jura Kruchkov, and Robert-Jan Slager, Non-Hermitian boundary modes and topology, *Phys. Rev. Lett.* **124**, 056802 (2020).
- [23] N. Okuma, K. Kawabata, K. Shiozaki, and M. Sato, Topological origin of non-Hermitian skin effects, *Phys. Rev. Lett.* **124**, 086801 (2020).
- [24] K. Zhang, Z. Yang, and C. Fang, Correspondence between winding numbers and skin modes in non-Hermitian systems, *Phys. Rev. Lett.* **125**, 126402 (2020).
- [25] P. W. Anderson, Absence of diffusion in certain random lattices, *Phys. Rev.* **109**, 1492 (1958).
- [26] J. Li, R.-L. Chu, J. K. Jain, and S.-Q. Shen, Topological Anderson insulator, *Phys. Rev. Lett.* **102**, 136806 (2009).
- [27] C. W. Groth, M. Wimmer, A. R. Akhmerov, J. Tworzydło, and C. W. J. Beenakker, Theory of the topological Anderson insulator, *Phys. Rev. Lett.* **103**, 196805 (2009).
- [28] Y. Xing, L. Zhang, and J. Wang, Topological Anderson insulator phenomena, *Phys. Rev. B* **84**, 035110 (2011).
- [29] H. Jiang, L. Wang, Q.-F. Sun, and X. C. Xie, Numerical study of the topological Anderson insulator in HgTe/CdTe quantum wells, *Phys. Rev. B* **80**, 165316 (2009).
- [30] Y.-Y. Zhang, R.-L. Chu, F.-C. Zhang, and S.-Q. Shen, Localization and mobility gap in the topological Anderson insulator, *Phys. Rev. B* **85**, 035107 (2012).
- [31] J. Song, H. Liu, H. Jiang, Q.-F. Sun, and X. C. Xie, Dependence of topological Anderson insulator on the type of disorder, *Phys. Rev. B* **85**, 195125 (2012).
- [32] A. Atland, D. Bagrets, L. Fritz, A. Kamenev, and H. Schmiedt, Quantum criticality of quasi-one-dimensional topological Anderson insulators, *Phys. Rev. Lett.* **112**, 206602 (2014).
- [33] I. Mondragon-Shem and T. L. Hughes, Topological criticality in the chiral-symmetric AIII class at strong disorder, *Phys. Rev. Lett.* **113**, 046802 (2014).
- [34] Z.-Q. Zhang, B.-L. Wu, J. Song, and H. Jiang, Topological Anderson insulator in electric circuits, *Phys. Rev. B* **100**, 184202 (2019).
- [35] H.-C. Hsu and T.-W. Chen, Topological Anderson insulating phases in the long-range Su-Schrieffer-Heeger model, *Phys. Rev. B* **102**, 205425 (2020).
- [36] G.-G. Liu, et al. Topological Anderson insulator in disordered photonic crystals, *Phys. Rev. Lett.* **125**, 133603 (2020).
- [37] S. Velury, B. Bradlyn, and T. L. Hughes, Topological crystalline phases in a disordered inversion-symmetric chain, *Phys. Rev. B* **103**, 024205 (2021).
- [38] G.-Q. Zhang, L.-Z. Tang, L.-F. Zhang, D.-W. Zhang, and S.-L. Zhu, Connecting topological Anderson and Mott insulators in disordered interacting fermionic systems, *Phys. Rev. B* **104**, L161118 (2021).
- [39] Z. Lu, Z. Xu, and Y. Zhang, Exact mobility edges

- and topological Anderson insulating phase in a slowly varying quasiperiodic model, *Ann. Phys. (Berlin)* **534**, 2200203, (2022).
- [40] M. Ren, et al. Realization of gapped and ungapped photonic topological Anderson insulators, *Phys. Rev. Lett.* **132**, 066602 (2024).
- [41] X.-D. Chen, et al. Realization of time-reversal invariant photonic topological Anderson insulators, *Phys. Rev. Lett.* **133**, 133802 (2024).
- [42] R. Ji, Y. Zhang, S. Chen, and Z. Xu, Controllable emergence of multiple topological Anderson insulator phases in photonic Su-Schrieffer-Heeger lattices, [arXiv:2512.06851](https://arxiv.org/abs/2512.06851).
- [43] T. Liu and H. Guo, Topological phase transition in the quasiperiodic disordered Su-Schrieffer-Heeger chain, *Physics Letters A* **382**, 3287 (2018).
- [44] S. Longhi, Topological Anderson phase in quasi-periodic waveguide lattices, *Optics Letters* **45**, 4036 (2020).
- [45] L.-Z. Tang, S.-N. Liu, G.-Q. Zhang, and D.-W. Zhang, Topological Anderson insulators with different bulk states in quasiperiodic chains, *Phys. Rev. A* **105**, 063327 (2022).
- [46] Li. et al., Mapping the topology-localization phase diagram with quasiperiodic disorder using a programmable superconducting simulator, *Phys. Rev. Research* **6**, L042038 (2024).
- [47] S. Sircar, Topological Anderson insulator phases in one dimensional quasi-periodic mechanical SSH chains, *Physics Letters A* **537**, 130314 (2025).
- [48] X. Wang, L. Wang, and S. Chen, Topological Anderson insulator and reentrant topological transitions in a mosaic trimer lattice, [arXiv:2601.13760](https://arxiv.org/abs/2601.13760).
- [49] N. Hatano and D. R. Nelson, Localization transitions in non-Hermitian quantum mechanics, *Phys. Rev. Lett.* **77**, 570 (1996).
- [50] N. M. Shnerb and D. R. Nelson, Winding numbers, complex currents, and non-Hermitian localization, *Phys. Rev. Lett.* **80**, 5172 (1998).
- [51] Z. Gong, Y. Ashida, K. Kawabata, K. Takasan, S. Higashikawa, and M. Ueda, Topological phases of non-Hermitian systems, *Phys. Rev. X* **8**, 031079 (2018).
- [52] S. Longhi, Topological phase transition in non-Hermitian quasicrystals, *Phys. Rev. Lett.* **122**, 237601 (2019).
- [53] S. Longhi, Metal-insulator phase transition in a non-Hermitian Aubry-André-Harper model, *Phys. Rev. B* **100**, 125157 (2019).
- [54] H. Jiang, L.-J. Lang, C. Yang, S.-L. Zhu, and S. Chen, Interplay of non-Hermitian skin effects and Anderson localization in nonreciprocal quasiperiodic lattices, *Phys. Rev. B* **100**, 054301 (2019).
- [55] Q.-B. Zeng and Y. Xu, Winding numbers and generalized mobility edges in non-Hermitian systems, *Phys. Rev. Research* **2**, 033052 (2020).
- [56] Y. Liu, Y. Wang, X. J. Liu, Q. Zhou, and S. Chen, Exact mobility edges, PT-symmetry breaking, and skin effect in one-dimensional non-Hermitian quasicrystals, *Phys. Rev. B* **103**, 014203 (2021).
- [57] X. Cai, Localization and topological phase transitions in non-Hermitian Aubry-André-Harper models with p-wave pairing, *Phys. Rev. B* **103**, 214202 (2021).
- [58] W. Chen, et al., Breakdown of the correspondence between the real-complex and delocalization-localization transitions in non-Hermitian quasicrystals, *Phys. Rev. B* **106**, 144208 (2022).
- [59] Q. Lin, et al., Topological phase transitions and mobility edges in non-Hermitian quasicrystals, *Phys. Rev. Lett.* **129**, 113601 (2022).
- [60] X. Q. Sun and C. S. Liu, Localization and topological transitions in generalized non-Hermitian SSH models, *Physics Letters A* **482**, 129043 (2023).
- [61] D.-W. Zhang, L.-Z. Tang, L.-J. Lang, H. Yan, and S.-L. Zhang, Non-Hermitian topological Anderson insulators, *Sci. China-Phys. Mech. Astron.* **63**, 267062 (2020).
- [62] H. Liu, Z. Su, Z.-Q. Zhang, and H. Jiang, Topological Anderson insulator in two-dimensional non-Hermitian systems, *Chinese Phys. B* **29**, 050502 (2020).
- [63] L.-Z. Tang, L.-F. Zhang, G.-Q. Zhang, and D.-W. Zhang, Topological Anderson insulators in two-dimensional non-Hermitian disordered systems, *Phys. Rev. A* **101**, 063612 (2020).
- [64] Q. Lin, T. Li, L. Xiao, K. Wang, W. Yi, and P. Xue, Observation of non-Hermitian topological Anderson insulator in quantum dynamics, *Nat. Commun.* **13**, 3229 (2022).
- [65] S. Aubry and G. André, *Ann. Isr. Phys. Soc.* **3**, 133 (1980).
- [66] P. G. Harper, Single band motion of conduction electrons in a uniform magnetic field, *Proc. Phys. Soc. A* **68**, 874 (1955).
- [67] S. Das Sarma, S. He, and X. C. Xie, Mobility edge in a model one-dimensional potential, *Phys. Rev. Lett.* **61**, 2144 (1988).
- [68] F. M. Izrailev and A. A. Krokhin, Localization and the mobility edge in one-dimensional potentials with correlated disorder, *Phys. Rev. Lett.* **82**, 4062 (1999).
- [69] S. Ganeshan, J. H. Pixley, and S. Das Sarma, Nearest neighbor tight binding models with an exact mobility edge in one dimension, *Phys. Rev. Lett.* **114**, 146601 (2015).
- [70] X. Deng, S. Ray, S. Sinha, G. V. Shlyapnikov, and L. Santos, One-dimensional quasicrystals with power-law hopping, *Phys. Rev. Lett.* **123**, 025301 (2019).
- [71] Y. Wang, X. Xia, L. Zhang, H. Yao, S. Chen, J. You, Q. Zhou, and X.-J. Liu, One-dimensional quasiperiodic mosaic lattice with exact mobility edges, *Phys. Rev. Lett.* **125**, 196604 (2020).
- [72] T. T. Geisel and G. Petschel, New class of level statistics in quantum systems with unbounded diffusion, *Phys. Rev. Lett.* **66**, 1651 (1991).
- [73] S. Y. Jitomirskaya, Metal-insulator transition for the almost mathieu operator, *Ann. Math.* **3**, 150 (1999).
- [74] T. C. Halsey, M. H. Jensen, L. P. Kadanoff, I. Procaccia, and B. I. Shraiman, Fractal measures and their singularities: The characterization of strange sets, *Phys. Rev. A* **33**, 1141 (1986).
- [75] A. D. Mirlin, Y. V. Fyodorov, A. Mildenerger, and F. Evers, Exact relations between multifractal exponents at the Anderson transition, *Phys. Rev. Lett.* **97**, 046803 (2006).
- [76] Y. Wang, C. Cheng, X.-J. Liu, and D. Yu, Many-body critical phase: extended and nonthermal, *Phys. Rev. Lett.* **126**, 080602 (2021).
- [77] Y. Wang, L. Zhang, S. Niu, D. Yu, and X.-J. Liu, Realization and detection of nonergodic critical phases in an optical Raman lattice, *Phys. Rev. Lett.* **125**, 073204 (2020).
- [78] T. Xiao, D. Xie, Z. Dong, T. Chen, W. Yi, and B.

- Yan, Observation of topological phase with critical localization in a quasi-periodic lattice, *Sci. Bull.* **66**, 2175 (2021).
- [79] H. Li, et al. Observation of critical phase transition in a generalized Aubry-André-Harper model with superconducting circuits, *npj Quantum Inf* **9**, 40 (2023).
- [80] A. Pal and D. A. Huse, Many-body localization phase transition, *Phys. Rev. B* **82**, 174411 (2010).
- [81] R. Nandkishore and D. A. Huse, Many-body localization and thermalization in quantum statistical mechanics, *Annu. Rev. Condens. Matter Phys.* **6**, 15 (2015).
- [82] A. Purkayastha, S. Sanyal, A. Dhar, and M. Kulkarni, Anomalous transport in the Aubry-André-Harper model in isolated and open systems, *Phys. Rev. B* **97**, 174206 (2018).
- [83] D. A. Abanin, E. Altman, I. Bloch, and M. Serbyn, Colloquium: Many-body localization, thermalization, and entanglement, *Rev. Mod. Phys.* **91**, 021001 (2019).
- [84] L.-J. Lang, X. Cai, and S. Chen, Edge states and topological phases in one-dimensional optical superlattices, *Phys. Rev. Lett.* **108**, 220401 (2012).
- [85] Y. E. Kraus, Y. Lahini, Z. Ringel, M. Verbin, and O. Zeitlinger, Topological states and adiabatic pumping in quasicrystals, *Phys. Rev. Lett.* **109**, 106402 (2012).
- [86] Y. E. Kraus and O. Zeitlinger, Topological equivalence between the Fibonacci quasicrystal and the Harper model, *Phys. Rev. Lett.* **109**, 116404 (2012).
- [87] S. Ganeshan, K. Sun, and S. Das Sarma, Topological zero-Energy modes in gapless commensurate Aubry-André-Harper models, *Phys. Rev. Lett.* **110**, 180403 (2013).
- [88] X. Cai, L.-J. Lang, S. Chen, and Y. Wang, Topological superconductor to Anderson localization transition in one-dimensional incommensurate lattices, *Phys. Rev. Lett.* **110**, 176403 (2013).
- [89] J. Wang, X.-J. Liu, G. Xianlong, and H. Hu, Phase diagram of a non-Abelian Aubry-André-Harper model with p-wave superfluidity, *Phys. Rev. B* **93**, 104504 (2016).
- [90] Q.-B. Zeng, S. Chen, and R. Lü, Generalized Aubry-André-Harper model with p-wave superconducting pairing, *Phys. Rev. B* **94**, 125408 (2016).
- [91] Q.-B. Zeng, Y.-B. Yang, and Y. Xu, Topological phases in non-Hermitian Aubry-André-Harper models, *Phys. Rev. B* **101**, 020201(R) (2020).
- [92] Q.-B. Zeng and R. Lü, Topological phases and Anderson localization in off-diagonal mosaic lattices, *Phys. Rev. B* **104**, 064203 (2021).
- [93] Q.-B. Zeng and R. Lü, Real spectra and phase transition of skin effect in nonreciprocal systems, *Phys. Rev. B* **105**, 245407 (2022).
- [94] A. Mostafazadeh, Pseudo-Hermiticity versus PT symmetry: The necessary condition for the reality of the spectrum of a non-Hermitian Hamiltonian, *J. Math. Phys.* **43**, 205 (2002).
- [95] Q.-B. Zeng, Y.-B. Yang, and R. Lü, Topological phases in one-dimensional nonreciprocal superlattices, *Phys. Rev. B* **101**, 125418 (2020).
- [96] F. Evers and A. D. Mirlin, Anderson transitions, *Rev. Mod. Phys.* **80**, 1355 (2008).
- [97] H. Weyl, Ueber die gleichverteilung von zahlen mod. eins, *Math. Ann.* **77**, 313 (1916).
- [98] G. H. Choie, Ergodicity and irrational rotations, *Proc. R. Ir. Acad., Sect. A* **93A**, 193 (1993).
- [99] F. Song, S. Yao, and Z. Wang, Non-Hermitian topological invariants in real space, *Phys. Rev. Lett.* **123**, 246801 (2019).
- [100] A. Avila, Global theory of one-frequency Schrödinger operators, *Acta. Math.* **1**, 215 (2015).
- [101] X.-C. Zhou, Y. Wang, T. J. Poon, Q. Zhou, and X.-J. Liu, Exact new mobility edges between critical and localized states, *Phys. Rev. Lett.* **131**, 176401 (2023).
- [102] A. Avila, S. Jitomirskaya, and C. A. Marx, Spectral theory of extended Harper's model and a question by Erdős and Szekeres, *Inventiones Mathematicae* **210**, 283 (2017).
- [103] B. Simon and T. Spencer, Trace class perturbations and the absence of absolutely continuous spectra, *Commun. Math. Phys.*, **125**, 113 (1989).
- [104] S. Jitomirskaya and C. A. Marx, Analytic quasi-periodic cocycles with singularities and the Lyapunov exponent of extended Harper's model, *Commun. Math. Phys.* **316**, 237 (2012).